Particle Generation in a Chemical Vapor Deposition Process with Seed Particles

The formation of aerosol particles by gas-phase chemical reaction in the presence of seed particles has been studied experimentally and theoretically. Titanium tetraisopropoxide (TTIP) vapor containing ultrafine TiO_2 seed particles was introduced into a laminar flow aerosol reactor, and the properties of produced TiO_2 aerosol were measured. By comparing the particle numbers and size distributions of the resulting aerosol with those of the seed particles and those of homogeneously nucleated particles in the absence of seed particles, the effects of initial concentrations of TTIP vapor, reaction temperatures, and properties of seed particles on the suppression of homogeneous nucleation were experimentally clarified. In the theoretical analysis, the population balance equation expressing simultaneous generation of TiO_2 monomer, Brownian coagulation and diffusive deposition of TiO_2 monomer and aerosols was solved. The observed suppression of homogeneous nucleation by the seed particles is explained qualitatively by the theoretical analysis.

Kikuo Okuyama
Ryuichi Ushio
Yasuo Kousaka
Department of Chemical Engineering
University of Osaka Prefecture
Sakai, Osaka 591 Japan

Richard C. Flagan
Department of Environmental
Engineering Science

John H. Seinfeld
Department of Chemical Engineering
California Institute of Technology
Pasadena, CA 91125

Introduction

Preparation of fine particles of diameters less than 0.1 μm by gas-phase chemical reaction is becoming an important technology as fine particles offer excellent possibilities as raw materials for ceramic materials, catalyst powders, and electronic devices. Chemical vapor deposition (CVD) techniques can be developed to produce fine particles in a gas phase as well as to produce thin films. CVD production of fine particles offers the following advantages:

- Particles produced are of high purity.
- Control of particle size is feasible.
- A relatively simple apparatus is required.
- Particle crystal structure is controllable.
- Particles are produced rapidly.
- The process is continuous.

If seed particles are introduced into the CVD system, the seed particles can be coated by the vapor of the CVD product, and the resulting particles can be relatively monodisperse.

Fine particle production by gas-phase chemical reaction is based on a gas-to-particle conversion process, in which the nucleation can occur homogeneously and/or heterogeneously. Homogeneous nucleation occurs by a vapor depositing on its own clusters or embryos in the absence of foreign substances as seed particles. In the presence of seed particles, monomer vapor and cluster deposition onto the existing seed particles suppresses the formation of new particles. Heterogeneous nucleation or growth can occur even under a low degree of supersaturation, whereas homogeneous nucleation requires much higher supersaturation.

In previous papers (Warren et al., 1987; Nguyen et al., 1987), the influence of seed particles on the rate of homogeneous nucleation from a supersaturated vapor formed by the physical cooling of the hot vapor (physical vapor deposition, PVD) has been studied experimentally and theoretically. It has been found that seed particles can decrease the homogeneous nucleation rate to an extent that depends on the seed particle number concentration and the generation rate of supersaturation by cooling. The suppression effect of existing seed particles on new particle formation by CVD, however, has not been clarified.

To evaluate the role of seed particles in the CVD process, the formation of fine particles by gas-phase chemical reaction in the presence of seed particles is studied experimentally and theoretically in the present paper using a laminar flow aerosol reactor (LFAR). As a model study of particle formation in a CVD process, the preparation of ultrafine titanium dioxide particles by the thermal decomposition of titanium tetraisopropoxide

Correspondence concerning this paper should be addressed to K. Okuyama.

(TTIP) vapor containing titanium dioxide seed particles was carried out using a well-controlled LFAR. Dry nitrogen gas with TTIP vapor, either particle-free or containing a seed aerosol, was introduced into the LFAR, and the resulting number concentrations of aerosol particles were measured under various conditions of vapor and seed particle properties. The effect of homogeneous nucleation suppression on the properties of the particles produced under various initial vapor concentrations, reaction rates, properties of seed particles and temperature profiles of the reactor were examined. A theoretical analysis of aerosol nucleation and growth in a laminar pipe flow is presented; in particular, particle formation by CVD in the LFAR was analyzed by numerically solving the aerosol general dynamic equation for chemical reaction, Brownian coagulation and diffusive deposition, and the predicted particle properties are compared with those observed.

Generation of Ultrafine Particles by Gas-Phase Chemical Reaction

Experimental apparatus and method

Figure 1 shows the experimental apparatus for generating ultrafineTiO_2 particles. The experimental system consists of drying columns, a deoxidizer, a vaporizer for titanium tetraisopropoxide vapor, a tubular reactor furnace, particle measurement system, and gas chromatograph. This system is similar to that used by Okuyama et al. (1986, 1988) with the addition of the generation system for ultrafine seed TiO_2 particles.

TTIP liquid was maintained in a heated glass vaporizer serving as the vapor source. The temperature of the vaporizer was varied between 30 and 50°C. Clean and dried nitrogen gas was used as a carrier gas and was passed through the vaporizer to be saturated with the TTIP vapor at the flow rate $Q1$. The stream was then mixed with either particle-free nitrogen gas or ultrafine seed aerosol having the flow rate $Q2$. In the reactor furnace, the TTIP vapor is thermally decomposed to produce titanium dioxide vapor by:

$$Ti(OC_3H_7)_4 \rightarrow TiO_2 + 4C_3H_6 + 2H_2O \qquad (1)$$

Since the saturation vapor pressure of TiO_2 is extremely low, the TiO_2 vapor produced attains a highly supersaturated state. This supersaturated vapor produces TiO_2 particles through homogeneous nucleation or leads to growth of the seed particles by heterogeneous condensation. In the case in which the supersaturation ratio of TiO_2 vapor is extremely high, the particle formation process is controlled by collisions among monomers and/or clusters. The existing seed particles will grow by the simultaneous condensation of vapor molecules and their coagulation with clusters.

The tubular furnace, the laminar flow aerosol reactor, used in the experiment consists of a 11.5-mm-ID high-quality stainless steel tube of about 550-mm length. The reactor has five heating zones, each 100 mm in length, separated by about 10 mm of low density insulation. Each of the heating zones was controlled carefully by a temperature controller to within ±2°C, $T1$, $T2$, $T3$, $T4$, and $T5$ indicate the controlled wall temperature of the heating zones along the LFAR. Since the furnace temperatures govern the rate of thermal decomposition of the TTIP vapor and the subsequent TiO_2 particle formation, the temperature profile was changed to study the effect of reaction temperature on the process. To prevent thermophoretic deposition of the small particles suspended in the hot carrier gas flow onto the cool wall of the sampling system, the aerosol stream was diluted by transpiring room temperature N_2 gas at a flow rate denoted by $Q3$ through a porous tube of length of about 100 mm, as used by

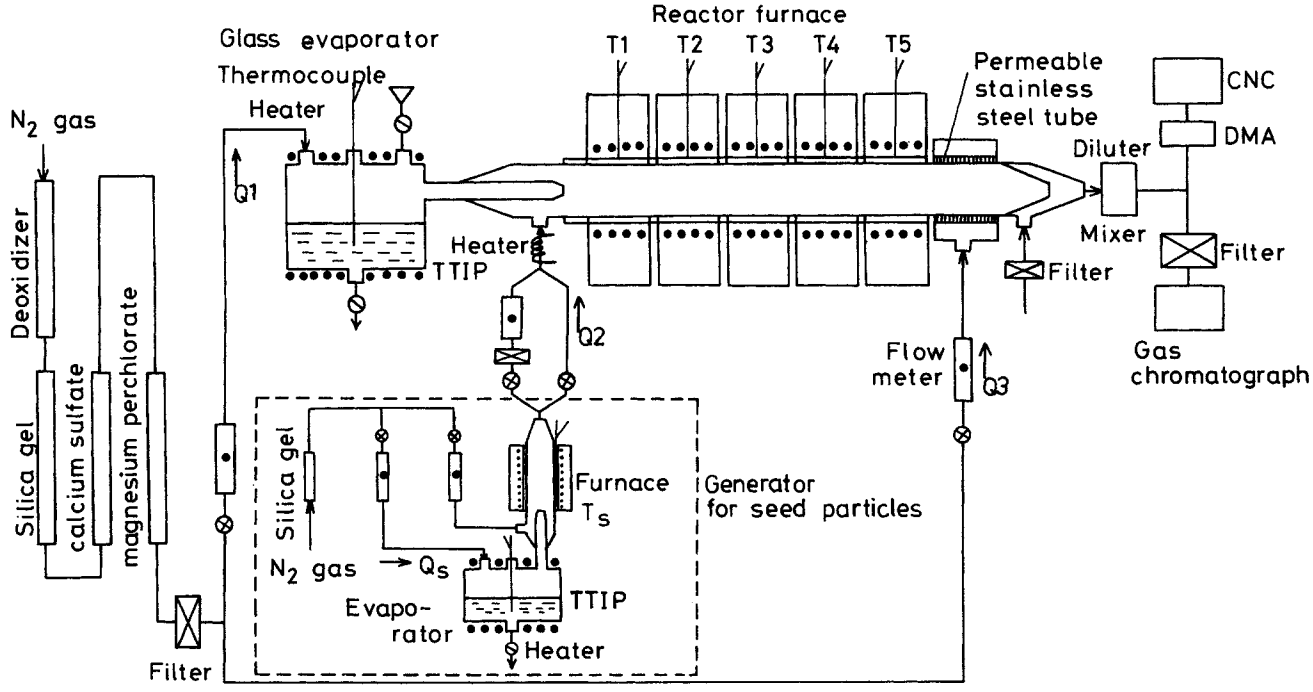

Figure 1. Experimental apparatus for generating ultrafine TiO_2 particles.

Wu and Flagan (1986). In the mixing of the seed aerosol with TTIP vapor and the gas mixture at the inlet of the furnace, the number concentrations of the TiO_2 seed particles were varied by dilution.

As indicated in Figure 1, the generation of seed particles involves a separate vaporizer to produce the TTIP vapor and a separate furnace to thermally decompose the TTIP vapor at a temperature of about 600°C. The sizes of seed aerosol were varied by controlling the flow rate of the TTIP vapor.

The analysis of particle size and number concentration of TiO_2 particles in the reactor outlet was carried out by two different methods as described by Okuyama et al. (1986). Particle size distributions were determined by electrostatic size analysis using a differential mobility analyzer (DMA), and the number concentration of the classified aerosol was measured by means of a mixing-type condensation nucleus counter (CNC). The electrical mobility distribution thus obtained was inverted to obtain the particle size distribution. The total particle number concentration was counted independently by a condensation nucleus counter (CNC) after the aerosol was diluted by nitrogen gas. The minimum detectable particle size by this method is about 0.003 μm in diameter.

A series of experiments was initiated by the homogeneous nucleation (no seed particles) experiment, namely the nitrogen gas flow carrying the TTIP vapor was set to the desired flow rate $Q1$, and the temperatures of the furnace, $T1$ to $T5$, were increased gradually. Once steady-state conditions were achieved, the number concentration and size distribution of homogeneously nucleated TiO_2 particles were measured. Then the heterogeneous condensation (with seed particles) experiment followed, in which the polydisperse TiO_2 seed particles were mixed with the TTIP feed vapor. The resulting number concentrations and size distributions of the TiO_2 aerosol produced by the combination of heterogeneous growth of seed particles and homogeneous nucleation were also monitored with DMA and CNC.

Experimental results

Figure 2 shows the size distribution of TiO_2 particles used as the seed particles for heterogeneous growth experiments. To produce seed particles, the TTIP vapor was generated at 40°C and the flow rates of the carrier gas, Q_s, were 60, 80 and 100 $cm^3 \cdot min^{-1}$. The nitrogen gas was added to maintain a total flow rate in the furnace of 700 $cm^3 \cdot min^{-1}$. The temperature of the furnace, T_s, was maintained at 600°C. Since N_s is the total seed particle number concentration per unit volume of gas and ρ is the gas density, N_s/ρ indicates the total seed particle number concentration per unit mass of dry gas. It is seen that TiO_2 seed particles increase in size as the initial concentration of TTIP vapor, C_A, is increased. This tendency was also seen in previous experimental results (Okuyama et al., 1986, 1989).

Figures 3–5 show the total number concentration of particles resulting from homogeneous nucleation and heterogeneous growth, N_f, at the outlet of the LFAR as a function of the number concentration of the TiO_2 seed particles, N_s. The values of d_{pg} and σ_g show the geometric mean diameter and standard deviation of TiO_2 particles formed by only homogeneous nucleation in the absence of seed particles, Figures 3 to 5.

In Figure 3, polydisperse seed particles having a geometric mean diameter d_{pgs} of 53.3 nm and a geometric standard

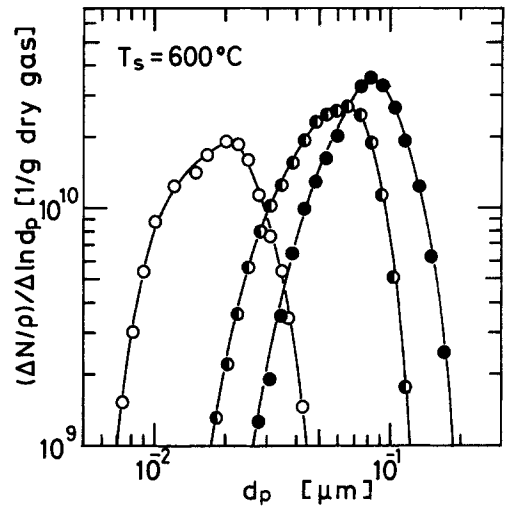

Key	Q_s [cc/min]	C_{A0} [mol/cc]	d_{pgs} [nm]	σ_{gs} [−]	$\bar{N}_s/\rho$ [1/g dry gas]
○	60	9.16×10^{-10}	18.1	1.48	1.96×10^{10}
◐	80	1.22×10^{-9}	53.3	1.49	2.68×10^{10}
●	100	1.53×10^{-9}	77.8	1.45	3.09×10^{10}

Figure 2. Size distribution of TiO_2 seed particles.

deviation σ_{gs} of 1.49 were used, and the temperature profile of the reactor furnace was changed to vary the thermal decomposition rate of TTIP vapor. The dashed curve corresponds to the experimental particle number concentration, N_{J0}, produced by homogeneous nucleation only in the absence of seed particles at

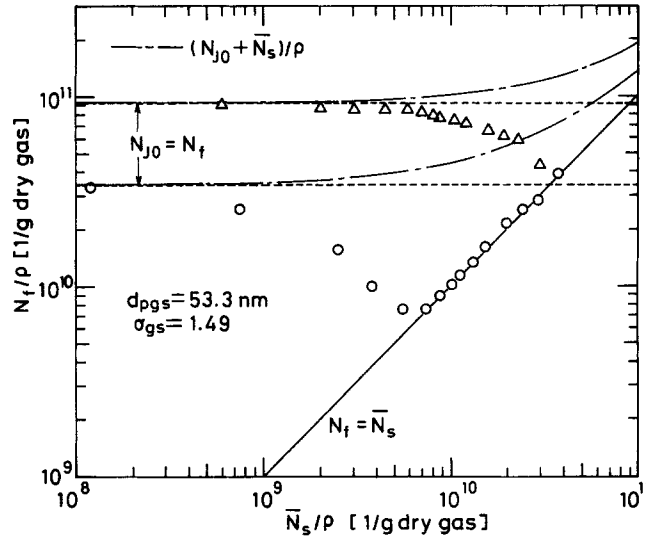

Key	T1	T2	T3	T4	T5 [°C]	d_{pg} [nm]	σ_g [−]	N_{J0}/ρ [1/g dry gas]
○	50	100	200	400	600	8.4	1.31	3.45×10^{10}
△	500	500	500	500	500	25.5	1.61	9.18×10^{10}

Figure 3. Measured total number concentration, N_f, produced in the aerosol reactor as a function of seed particle number concentration, N_s, under uniform or varying temperature profile in the furnace.

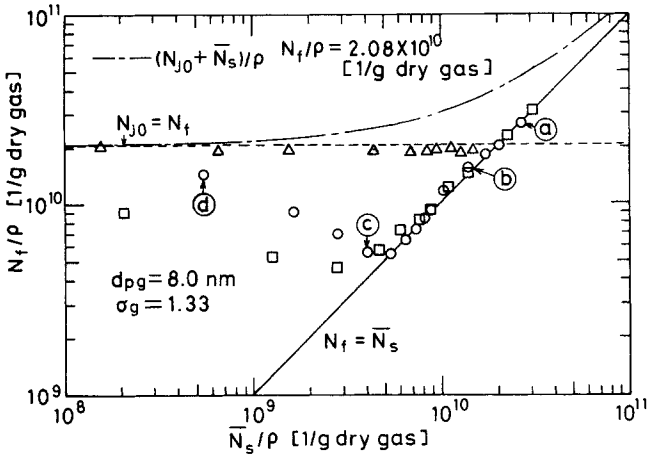

Key	T1 T2 T3 T4 T5 [°C]	dpgs [nm]	σgs [−]
△		18.1	1.48
○	50 100 200 400 600	53.3	1.49
□		77.8	1.45

Figure 4. Measured total number concentration, N_f, produced in the aerosol reactor as a function of seed particle number concentration, N_s, for different seed particle sizes.

the given conditions. The solid line indicates the relationship that holds if the number concentration of particles produced is equal to that of seed particles introduced: that is, homogeneous nucleation does not produce any new particles. Single dashed curves represent the total number concentration of particles produced assuming that homogeneous nucleation is not influenced by the existence of seed particles, which are labeled $(N_{J0} + N_s)/\rho$. The sum of homogeneously nucleated particles and seed particles is equal to the total particles at the reactor outlet.

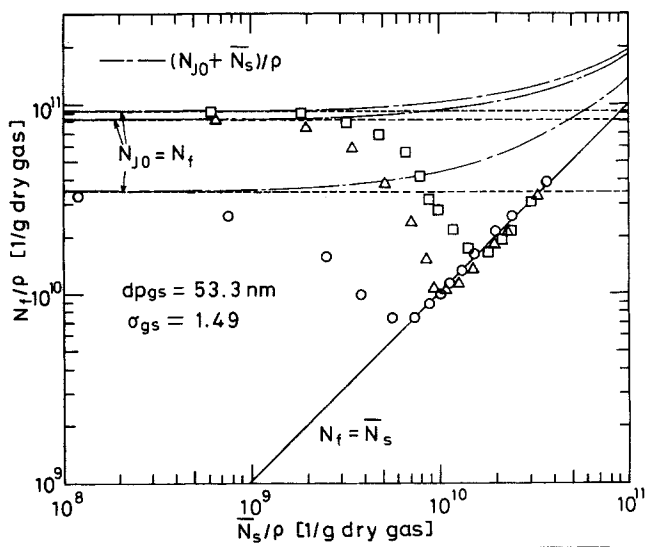

Key	T1 T2 T3 T4 T5 [°C]	C_{A0} [mol/cc]	dpg [nm]	σg [−]	N_{J0}/ρ [1/g dry gas]
○		1.51×10^{-10}	8.4	1.31	3.45×10^{10}
△	50 100 200 400 600	2.24×10^{-10}	11.0	1.40	8.24×10^{10}
□		3.69×10^{-10}	15.2	1.49	9.18×10^{10}

Figure 5. Measured total number concentration, N_f, produced in the aerosol reactor as a function of seed particle number concentration, N_s, for different concentrations of TTIP vapor.

Comparison of the experimental data with single dashed curves shows that in this case homogeneous nucleation was suppressed by the introduction of the seed particles. The suppression of homogeneous nucleation is found to be affected by the temperature profile, that is, an increasing temperature profile can lead to homogeneous nucleation suppression more effectively than at a constant profile at the high temperature, because the thermal decomposition of TTIP is initiated more slowly in the former case. This behavior is expected since a lower furnace temperature results in a lower concentration of TiO_2 monomer, and the rate of homogeneous nucleation is extremely sensitive to this TiO_2 monomer concentration. We note that homogeneous nucleation was suppressed by the introduction of seed particles at concentrations exceeding about 1×10^9 (g dry gas)$^{-1}$. The fact that the number concentration of the seed nuclei is the critical factor in suppressing homogeneous nucleation is in good agreement with the results obtained on the physical cooling of hot vapor in the laminar flow aerosol generator (Nguyen et al., 1987).

Figure 4 shows the effect of seed particle size on homogeneous nucleation with an increasing temperature profile in the furnace. It is seen that larger seed particles have a greater effect on suppressing homogeneous nucleation. This behavior is reasonable since the amount of TiO_2 vapor scavenged by the seed particles is proportional to their surface area and the supersaturation ratio of TiO_2 vapor decreases accordingly. Thus, seed particle size is also found to be a critical factor in suppressing homogenous nucleation producing ultrafine particles.

The effect of the feed concentration of TTIP vapor on the suppression of homogeneous nucleation is shown in Figure 5. It is seen that the number concentration of TiO_2 particles produced by homogeneous nucleation, N_{J0}, tends to increase with the vapor concentration, C_{A0}. As the number concentration of particles formed by homogeneous nucleation tends to increase, a higher number concentration of seed particles is necessary to suppress homogeneous nucleation.

Figure 6 shows the size distributions of particles formed under the conditions corresponding to points, a, b, c, and d in Figure 4. Figure 7 shows the size distributions of seed particles introduced (denoted by O) and of homogeneously nucleated particles (denoted by O) in the absence of seed particles. It is of interest to compare the size distributions of particles between Figures 6 and 7. In both cases of points a and b as shown in Figures 6a and 6b, where the introduction of seed particles almost completely suppresses homogeneous nucleation, the particles are found to grow slightly by heterogeneous condensation. In the cases of c and d, where homogeneous nucleation occurs simultaneously with the growth of seed particles by heterogeneous condensation, it is seen that bimodal size distributions are produced. The smaller particles are those produced by homogeneous nucleation, and the larger particles are the seed particles grown by heterogeneous condensation. The average sizes of grown seed particles are 66.1 nm in Figure 6c and 81.0 nm in Figure 6d, respectively, and tend to increase with the decrease in their number concentrations, but the geometric standard deviations are unchanged. Since the original average size of seed particles

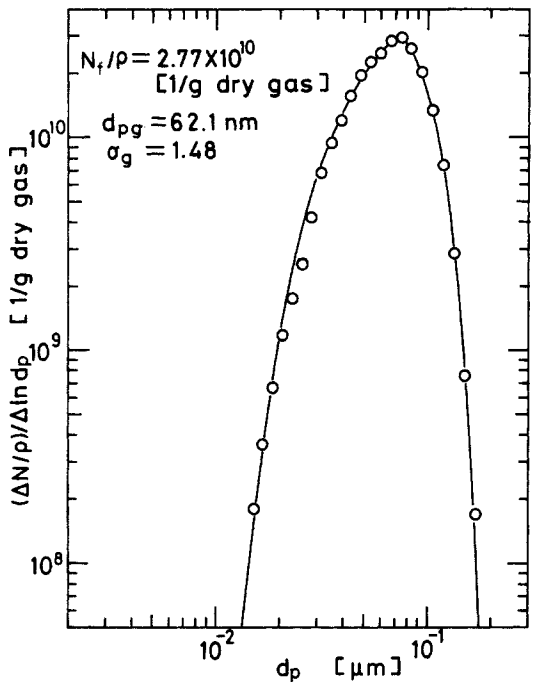

Figure 6a. Particle size distribution of particles produced corresponding to point a in Figure 4.

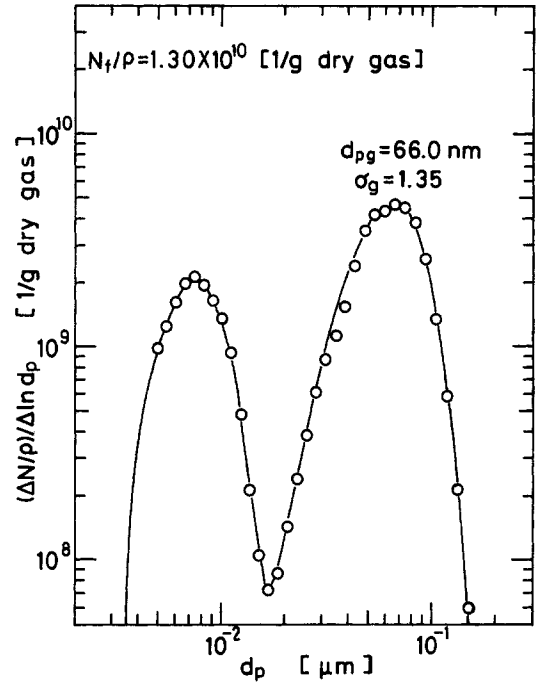

Figure 6c. Particle size distribution of particles produced corresponding to point c in Figure 4.

is 53.3 nm, about a 52% increase of average size has been accomplished in the case of Figure 6d.

Simulation of Aerosol Evolution in the Reactor Furnace

In the reactor furnace, the TTIP vapor is thermally decomposed to produce TiO_2 vapor. If the supersaturation ratio of TiO_2 reaches a sufficient level, ultrafine primary TiO_2 particles are formed by homogeneous nucleation. The thermal decomposition rate of TTIP vapor is rapid under the experimental conditions studied, the saturated vapor pressure of TiO_2 is very low, and the TiO_2 cluster and particles produced are solid-like with large surface tension. The evolution of larger secondary particles occurs as a result of cluster-cluster, cluster-particle and particle-

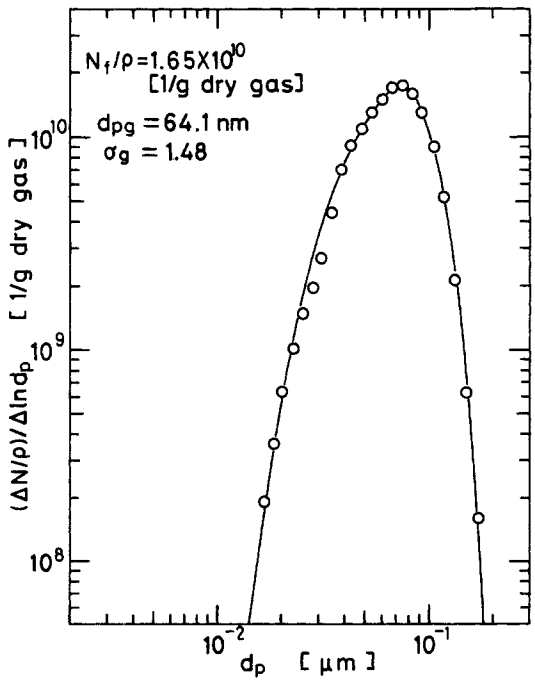

Figure 6b. Particle size distribution of particles produced corresponding to point b in Figure 4.

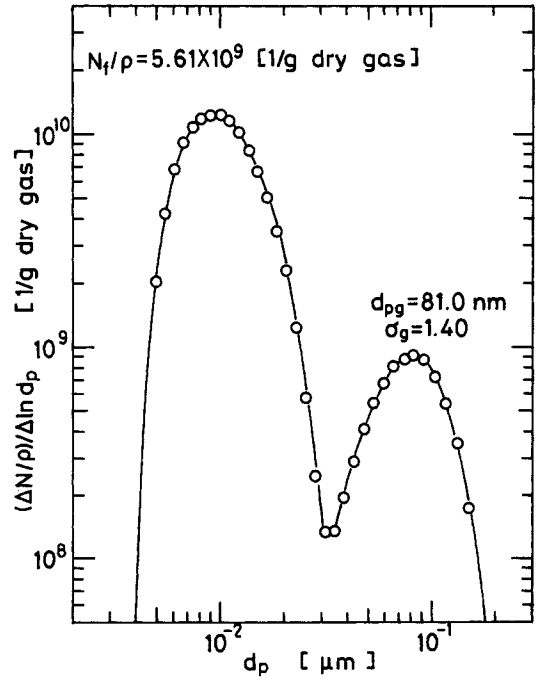

Figure 6d. Particle size distribution of particles produced corresponding to point d in Figure 4.

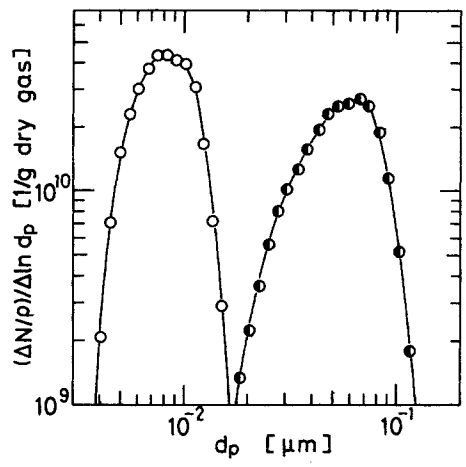

Homogeneously nucleated particles

Key	T1 T2 T3 T4 T5 [°C]	d_{pg} [nm]	σ_g [-]	N_{J0}/ρ [1/g dry gas]
○	50 100 200 400 600	8.0	1.33	3.45×10^{10}

Seed particles

Key	Ts [°C]	d_{pgs} [nm]	σ_{gs} [-]	$\bar{N}_s/\rho$ [1/g dry gas]
◐	600	53.3	1.49	2.68×10^{10}

Figure 7. Size distribution of homogeneously nucleated particles and seed particles.

particle collisions, or individual cluster and particle growth due to the accretion of vapor molecules. The evaporation of monomers from clusters and particles can be ignored.

The dynamic behavior of monomers, clusters and aerosol particles in the LFAR is described by the aerosol general dynamic equation (GDE) (Friedlander, 1977; Seinfeld, 1986). The so-called discrete-sectional GDE (Wu et al., 1988) is the most appropriate to evaluate the aerosol formation and growth under the present high source rate conditions. In the discrete-sectional GDE, the particle size spectrum is separated into two parts: the smaller clusters, the concentrations of which vary rapidly with time, are described by discrete number concentrations; and the larger clusters and particles are represented by continuous mass concentrations in sections. Whereas this discrete-sectional model is a detailed model of the evolution of the entire particle-size spectrum, the computational demands become severe in the case of nonuniform temperature, concentration and gas velocity in the LFAR.

Wu et al. (1988) developed a simplified reaction and coagulation model (SRC model), in which clusters in the discrete size spectrum and particles in the continuous size spectrum are lumped into a single mode. The evolution of the total cluster and particle concentrations can be evaluated by considering the intermode coagulation. As expected, this SRC model oversimplifies the evolution of clusters. Here the TiO_2 monomer is of a high saturation ratio, and small clusters (e.g., dimer and trimer) that result from the monomer clustering become significant. It is necessary, therefore, to extend the concept of the SRC model to include more discrete cluster sizes. The current size spectrum representation is similar to that of the discrete-sectional GDE, except that we use only one section to describe the particles (i.e., particles are approximated as monodisperse). Since this extended SRC model is computationally more appropriate for the current nonuniform system, the particle formation is analyzed by numerically solving the convective diffusion equation with the particle formation term based on the extended SRC model.

Basic conservation equations

In the extended SRC model, the particle size representation is assumed to be composed of four modes. The first mode follows the evolution of monomer. The second mode and the third mode represent clusters below k-mer and particles above $(k+1)$-mer, respectively. The fourth, called the seed mode, describes the evolution of the seed particles. Mass can be also added to the fine and seed particle modes. Monomer is produced by the chemical reaction source, and is removed by clusters and seed particles. Both the particle and the seed modes are monitored by the number and mass concentrations, N_p and M_p, and N_s and M_s, respectively. The monomer mode and the cluster mode are denoted by the number concentrations, N_m and N_ℓ, respectively. The TTIP vapor concentration is expressed by the molar concentration, C_v. In the laminar flow aerosol reactor, seed particles and molecules, clusters and particles tend to coagulate and diffuse due to Brownian motion.

The molar concentration of TTIP vapor, C_v, and the temperature T are governed by the convective diffusion equation and the thermal energy equation,

$$\nabla \cdot D_v \nabla \left(\frac{C_v}{\rho}\right) - \nabla \cdot u \left(\frac{C_v}{\rho}\right) - k_A \left(\frac{C_v}{\rho}\right) = 0 \tag{2}$$

$$\nabla \cdot \alpha \nabla T - \nabla \cdot uT = 0 \tag{3}$$

The population balance equations expressing the conservation of number concentrations of monomer and cluster, at steady state, are given by: (monomer number concentration : N_m)

$$\nabla \cdot D_m \nabla \left(\frac{N_m}{\rho}\right) - \nabla \cdot u \left(\frac{N_m}{\rho}\right) - \rho \sum_{j=1}^{k} \beta\,(v_m, v_j) \frac{N_m}{\rho} \frac{N_j}{\rho} - \rho\,\beta\,(v_m, v_p) \frac{N_m}{\rho} \frac{N_p}{\rho} - \rho\,\beta\,(v_m, v_s) \frac{N_m}{\rho} \frac{N_s}{\rho} + k_A \frac{C_v}{\rho} N_{AV} = 0 \tag{4}$$

(number concentration of clusters containing ℓ monomers $(2 \leq \ell \leq k)$:N_ℓ)

$$\nabla \cdot D_\ell \nabla \left(\frac{N_\ell}{\rho}\right) - \nabla \cdot u \left(\frac{N_\ell}{\rho}\right) + \frac{1}{2} \rho \sum_{j=1}^{\ell-1} \beta\,(v_{\ell-j}, v_j) \frac{N_{\ell-j}}{\rho} \frac{N_j}{\rho} - \rho \sum_{j=1}^{k} \beta(v_\ell, v_j) \frac{N_\ell}{\rho} \frac{N_j}{\rho} - \rho\,\beta(v_\ell, v_p) \frac{N_\ell}{\rho} \frac{N_p}{\rho} - \rho\,\beta(v_\ell, v_s) \frac{N_\ell}{\rho} \frac{N_s}{\rho} = 0 \tag{5}$$

where k is the cluster number cutoff in the discrete-size spectrum. The population balance equations expressing the conservation of number and mass concentrations of fine particles and seed particles are given by: *Number concentration of*

particles above $(k+1)$ *– mer:* N_p

$$\nabla \cdot D_p \nabla\left(\frac{N_p}{\rho}\right) - \nabla \cdot u\left(\frac{N_p}{\rho}\right) + \frac{1}{2}\rho \sum_{i=1}^{k}\sum_{j=1}^{k} \beta\,(v_{k+i-j}, v_j)\,\frac{N_{k+i-j}}{\rho}\frac{N_j}{\rho} - \frac{1}{2}\rho\,\beta\,(v_p, v_p)\left(\frac{N_p}{\rho}\right)^2 - \rho\,\beta(v_p, v_s)\,\frac{N_p}{\rho}\frac{N_s}{\rho} = 0 \quad (6)$$

Number concentration of seed particles: N_s

$$\nabla \cdot D_s \nabla\left(\frac{N_s}{\rho}\right) - \nabla \cdot u\left(\frac{N_s}{\rho}\right) - \frac{1}{2}\rho\,\beta(v_s, v_s)\left(\frac{N_s}{\rho}\right)^2 = 0 \quad (7)$$

Mass concentration of particles above dimers: M_p

$$\nabla \cdot D_p \nabla\left(\frac{M_p}{\rho}\right) - \nabla \cdot u\left(\frac{M_p}{\rho}\right) + \frac{1}{2} m_{k+1}\,\rho \sum_{i=1}^{k}\sum_{j=1}^{k} \beta(v_{k+i-j}, v_j)\,\frac{N_{k+1-j}}{\rho}\frac{N_j}{\rho} + \rho \sum_{j=1}^{k} m_j\,\beta(v_j, v_p)\,\frac{N_j}{\rho}\frac{N_p}{\rho} - \rho\,\beta(v_p, v_s)\,\frac{M_p}{\rho}\frac{N_s}{\rho} = 0 \quad (8)$$

Mass concentration of seed particles: M_s

$$\nabla \cdot D_s \nabla\left(\frac{M_s}{\rho}\right) - \nabla \cdot u\left(\frac{M_s}{\rho}\right) + \rho \sum_{j=1}^{k} m_j\,\beta(v_j, v_s)\,\frac{N_j}{\rho}\frac{N_s}{\rho} + \rho\,\beta(v_p, v_s)\,\frac{M_p}{\rho}\frac{M_s}{\rho} = 0 \quad (9)$$

The thermal decomposition of TTIP vapor in the reaction of Eq. 1 can be represented as first-order having the rate constant,

$$k_A = 3.96 \times 10^5 \exp\left(-7.05 \times 10^4 / R_g T\right), \text{ s}^{-1}$$

which was experimentally obtained by measuring the propylene gas concentration using a gas chromatograph as shown in the Appendix. This reaction rate constant is in in reasonably good agreement with that of Kanai et al. (1985).

The average diameters of monomer, ℓ-mer cluster, particles and seed particles are given by the following relations:

$$d_m = (6m_m/\pi\rho_p)^{1/3}, \quad m_m = 10^{-3}(m_w/N_{AV}), \quad d_\ell = (6\ell m_m/\pi\rho_p)^{1/3} \quad (10)$$

$$d_p = (6M_p/\pi\rho_p N_p)^{1/3}, \quad d_s = (6M_s/\pi\rho_p N_s)^{1/3} \quad (11)$$

Diffusion coefficients, D_m, D_ℓ, D_p, D_s, and D_v, are obtained from the Stokes-Cunningham equation:

$$D_i = (C_c k_B T/3\pi\,\mu d_i) \qquad i = m, \ell, p, s, v. \quad (12)$$

where C_c is the slip correction factor.

Let us consider Eq. 4 for the number concentration of monomer. The first term on the lefthand side of Eq. 4 accounts for the Brownian diffusion, the second term the transport due to laminar flow, the third term the rate of loss of monomer due to collision with clusters, the fourth term the loss of monomer due to collision with nucleated particles, the fifth term the loss of monomer due to collision with seed particles, and the sixth term the generation of monomer by the thermal decomposition of TTIP vapor.

At the reactor entry ($z = 0$), the carrier gas introduced is assumed to have the number and mass concentration of seed particles, N_{s0}, and M_{s0}, and the molar concentration of TTIP vapor, C_{v0}:

$$z = 0, \quad 0 \leqq r \leqq R; \quad N_m = N_p = M_p = 0, \quad N_s = N_{s0}, \quad M_s = M_{s0}, \quad C_v = C_{A0}, \quad T = T_0, \quad N_\ell = 0 \quad \text{for} \quad \ell = 1 \sim k \quad (13)$$

Boundary condtions are given by

$$r = 0; \quad \frac{\partial}{\partial r}\left(\frac{N_m}{\rho}\right) = \frac{\partial}{\partial r}\left(\frac{N_p}{\rho}\right) = \frac{\partial}{\partial r}\left(\frac{M_p}{\rho}\right) = \frac{\partial}{\partial r}\left(\frac{N_s}{\rho}\right) = \frac{\partial}{\partial r}\left(\frac{M_s}{\rho}\right) = \frac{\partial T}{\partial r} = 0 \quad \frac{\partial}{\partial r}\left(\frac{N_\ell}{\rho}\right) = 0 \quad \text{for} \quad \ell = 1 \sim k \quad (14)$$

$$r = R; \quad N_m = N_p = M_p = N_s = M_s = 0, \quad \frac{\partial}{\partial r}\left(\frac{C_v}{\rho}\right) = 0, \quad T = T_R \quad N_\ell = 0 \quad \text{for} \quad \ell = 1 \sim k \quad (15)$$

In the derivation of Eqs. 4–9, the following assumptions have been invoked:

1. At the reactor entry ($z = 0$), the parabolic velocity profile of gas u is already fully developed, and the effect of temperature on the velocity profile is negligible.
2. Particles are spherical and electrically neutral.
3. Particles collide with each other to form single new spherical particle whose mass is the same as the combined mass of the two smaller particles.
4. All particles colliding with the reactor wall are removed.
5. TTIP vapor molecules are not absorbed on the surface of the tube.
6. Brownian diffusion of monomer, clusters and particles in the axial direction can be neglected relative to convection.
7. Thermal diffusion and thermophoresis of particles can be neglected.
8. Heat generation by the reaction of the TTIP vapor decomposition or the heat of condensation of TiO_2 can be neglected.

For Brownian coagulation, the well known Fuchs interpolation formula in the transition regime (Fuchs, 1964) has been used. In this expression, the effect of the van der Waals force on the coagulation rate has not been included. Since both van der Waals forces and polydispersity will enhance Brownian coagulation over that predicted by the Fuchs formula, an enhancement factor W is included in the Fuchs formula to be determined by the comparison of simulations and observations (Okuyama et al., 1984).

Since Eqs. 2–9 cannot be solved analytically, the following numerical approximation method is employed to solve them. The set of simultaneous partial differential equations are approximated by finite difference formulas, and these equations are integrated by the Crank-Nicolson method. In order to ensure the accuracy of the numerical solutions, comparisons were made between numerical solutions with different step sizes, and most calculations were made with 51 radial and 6,000 axial points.

To determine an appropriate value of the cluster number cutoff in the discrete size spectrum k, numerical results obtained for different k values were compared. Since it was determined that k should be taken to be at least 5 in this comparison, we decided to use $k = 5$ in our subsequent simulation.

The numerical solution of Eqs. 4–9 gives the particle number concentration and mass concentration, and their average values in the axial plane at any distance z from the inlet:

$$N_{J0}/\rho = \int_0^{2x}\int_0^R (N_p/\rho)\, ur\, dr\, d\theta/Q_s$$

$$M_{J0}/\rho = \int_0^{2x}\int_0^R (M_p/\rho)\, ur\, dr\, d\theta/Q_s$$

$$\overline{N_s}/\rho = \int_0^{2x}\int_0^R (N_s/\rho)\, ur\, dr\, d\theta/Q_s$$

$$\overline{M_s}/\rho = \int_0^{2x}\int_0^R (M_s/\rho)\, ur\, dr\, d\theta/Q_s$$

$$N_f/\rho = \int_0^{2x}\int_0^R \{(N_p/\rho) + (N_s/\rho)\}\, ur\, dr\, d\theta/Q_s$$

$$M_f/\rho = \int_0^{2x}\int_0^R \{(M_p/\rho) + (M_s/\rho)\}\, ur\, dr\, d\theta/Q_s \qquad (16)$$

where

$$Q_s = \int_0^{2x}\int_0^R ur\, dr\, d\theta.$$

Since the particle number concentration of the product aerosol is that measured, N_{J0}, N_s and N_f at $z = L$ need to be calculated by Eq. 16. Furthermore, the mass deposition rates of monomer, ℓ-mer clusters, nucleated particles and seed particles on the reactor wall can be calculated by:

For TiO_2 monomer

$$M_w = \int_0^Z 2\pi\, Rm_m D_m(\partial N_m/\partial r)\, dz \quad \text{at} \quad r = R \qquad (17)$$

For ℓ-mer clusters ($2 \leq \ell \leq k$)

$$M_{w\ell} = \int_0^Z 2\pi\, R\ell m_m D_\ell(\partial N_\ell/\partial r)\, dz \quad \text{at} \quad r = R \qquad (18)$$

For nucleated TiO_2 particles and seed particles

$$M_{wi} = \int_0^Z 2\pi\, Rm_i D_i(\partial N_i/\partial r)\, dz$$

$$m_i = M_i/N_i \quad \text{at} \quad r = R, \quad \text{for} \quad i = p, s \qquad (19)$$

Simulations vs. observations

Figure 8 shows the comparison of measured and predicted particle number concentrations. The experimental points shown in Figures 8a, 8b and 8c correspond to those shown in Figures 3, 4 and 5, respectively. The dashed curves represent the simulation results corresponding to the experimental conditions. By matching the simulated particle behavior by homogeneous nucleation to fit the observed values, the enchancement factor W for the Brownian coagulation between monomer and monomer, monomer and particle, particle and particle, is determined to be about 5.0. This value is reasonable when compared with values of W ranging from 2 to 7 for ultrafine NaCl and Ag particles (Okuyama et al., 1984). For Brownian coagulation between seed particles, the enhancement factor W is assumed to be unity because of the larger size of those particles.

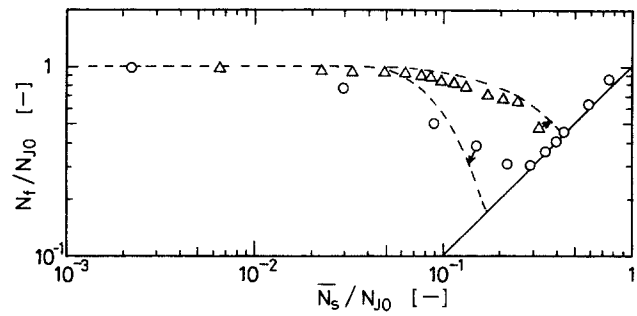

Figure 8a. Results simulated by extended SRC model vs. experimental data shown in Figure 3.

Since the simulated number concentration of particles, N_{J0}, produced by homogeneous nucleation in the absence of seed particles does not agree with the observed values, the comparison between the experiment and the simulation has been made by normalizing the values of N_f and N_s by N_{J0}. For example, in the case of Figure 3 with a constant temperature of 500°C, the simulated value of N_{J0} is 1.24×10^{11} (g dry gas)$^{-1}$ and the experimental value is 9.18×10^{10} (g dry gas)$^{-1}$. As seen from Figure 8a, the tendency to suppress homogeneous nucleation as a function of the rate of reaction is qualitatively explained by the simulation results. Larger seed particles produce larger suppression of homogeneous nucleation. This finding is in qualitative agreement with that predicted, Figure 8b. In Figure 8c, the effect of initial vapor concentration on the suppression tendency of homogeneous nucleation is also explained by the simulation. The deviation between the simulated and observed results shown in Figures 8a and 8b is caused primarily by the assumption that both the seed particles and the nucleated particles are monodisperse. The suppression is shown to be negligible for values of N_s/N_{J0}, less than about 0.01; and the growth of seed particles

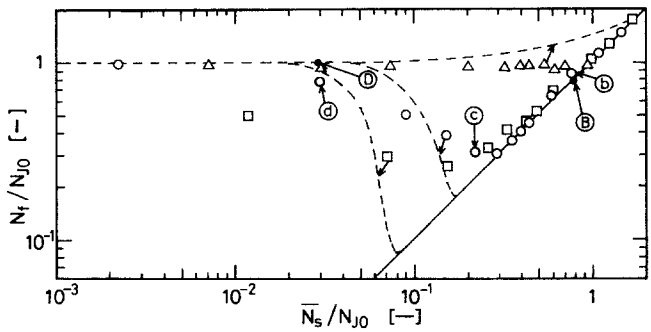

Figure 8b. Results simulated by extended SRC model vs. experimental data shown in Figure 4.

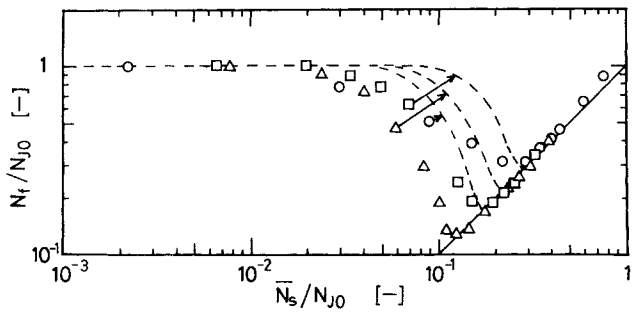

Figure 8c. Results simulated by extended SRC model vs. experimental data shown in Figure 5.

suppresses homogenous nucleation at values of N_s/N_{J0}, is larger than about 1.0

Implications for Design of Particle Production CVD Systems

The suppression of homogeneous nucleation by seed particles in a CVD-type reactor is found to depend on the number and size of seed particles, the rate of generation of monomer by chemical reaction, and the feed vapor concentration.

Figures 9, 10 and 11 show the calculated average number concentrations (N_v, $N_g + N_p$, and N_s), mass concentrations ($M_g + M_p$ and M_s), and volume-averaged diameters (d_p and d_s) along the reactor length, corresponding to the experimental conditions shown by the solid points B and D in Figure 8b. Figure 12 shows the calculated mass deposition rate onto the reactor wall. At point *B*, seed growth by heterogeneous condensation dominates particle formation, and point *D* corresponds to the homogeneous nucleation dominant condition. In Figure 9, which shows the changes in number concentration, it is seen that

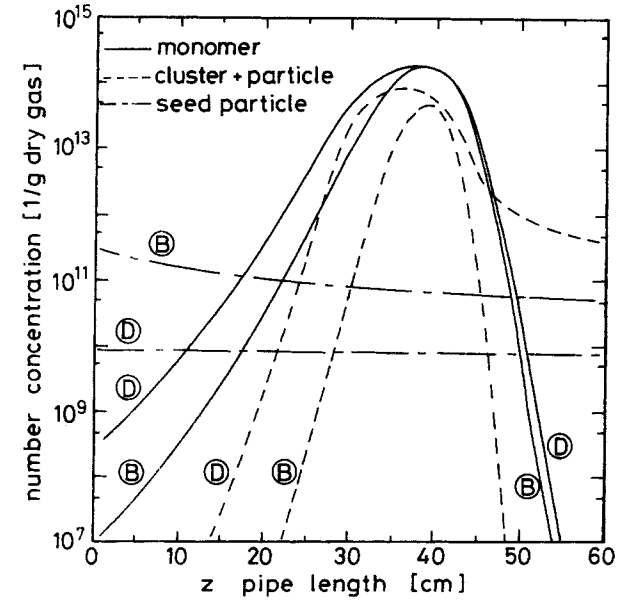

Figure 9. Calculated results of number concentration of monomer, homogeneously nucleated particles and seed particles as a function of reactor length corresponding to points B and D in Figure 8b.

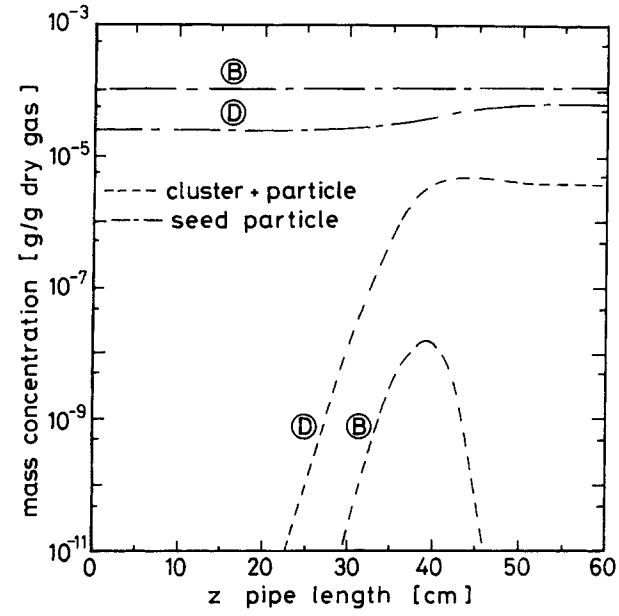

Figure 10. Calculated results of mass concentration of homogeneously nucleated particles and seed particles as a function of reactor length corresponding to points B and D in Figure 8b.

TiO_2 vapor molecules at first increase by the thermal decomposition of TTIP, and then particles begin to appear due to the coagulation of monomers. From the comparison between conditions *B* and *D*, we see that one order of magnitude difference in seed particle number concentration can produce a significant effect on the number concentration of monomers and particles. This is also clear in the changes in mass concentration shown in Figure 10. As seen from Figure 11, the final size of the seed

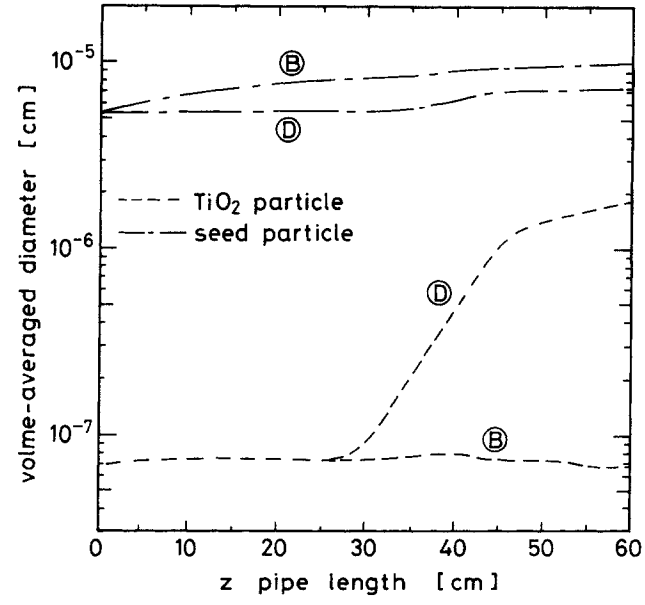

Figure 11. Calculated results of volume-averaged diameter of homogeneously nucleated particles and seed particles as a function of reactor length corresponding to points B and D in Figure 8b.

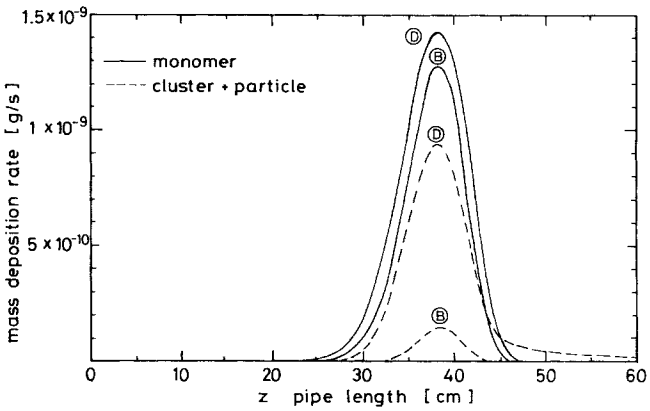

Figure 12. Calculated results of mass deposition of monomer and homogeneously nucleated particles as a function of a pipe length under the condition of points B and D in Figure 8b.

particles does not depend significantly on the conditions, which is in good agreement with the results of Figure 8. The slight decrease in the number concentration of seed particles in condition B of Figure 9 is the result of Brownian coagulation.

Adhesion of monomers, clusters and particles to seed particles tends to suppress homogeneous nucleation. When the temperature profile of the furnace is increasing, the monomer number concentration attains a maximum around the middle of the reactor, as seen from Figure 9, and the deposited mass of monomer and particles is found also to reach a maximum around the middle of the reactor from Figure 12, although the growth of seed particles clearly reduces the deposition of particles onto the reactor wall. The seed particles become an effective use of the limited amount of TiO_2 monomer vapor produced.

It is desirable to define the operating condition of the LFAR where the growth of the seed particles introduced becomes predominant. It is, however, difficult to classify the behavior of the LFAR using dimensionless parameters. At the present stage, only a qualitative indication can be made for determining the necessary conditions for producing a narrow or controlled size distribution. They are as follows:

- The number concentration of seed particles should be the order of that of homogeneously nucleated particles in the absence of seed particles.
- Larger seed particles can decrease the number concentration of seed particles necessary to suppress homogeneous nucleation.
- The chemical reaction producing the CVD product should be slow to suppress homogeneous nucleation.

Conclusion

The preparation of fine particles by chemical vapor deposition under the existence of seed particles in a laminar flow aerosol reactor has been studied experimentally and theoretically. Experimental results are quite consistent with those predicted using an extended simplified reaction and coagulation model. The introduction of seed particles—with the size range between 0.01 and 0.1 μm—into an aerosol reactor can decrease the homogeneous nucleation rate, depending on the seed particle size and number concentration. The suppression due to the seed particles is found to be higher: the higher the number concentration of seed particles, the larger their size. The suppression becomes negligible when the ratio of the number concentration of seed particles, N_s, to that of homogeneously nucleated particles in the absence of seed particles, N_{J0}, is less than about 0.01. On the other hand, the growth of seed particles can completely suppress homogeneous nucleation at values of N_s/N_{J0} larger than about 1.0. Seed particle size has a larger effect on the suppression of homogeneous nucleation as the size of seed particles becomes larger.

Acknowledgment

This work was supported by Japan Grant in Aid for Scientific Research No. 60750876.

Notation

C_{A0} = input concentration of metal alkoxide vapor into LFAR, mol/cm^3
C_c = slip correction factor
C_v = monomer concentration of metal alkoxide vapor, mol/cm^3
D = diffusion coefficient, cm^2/s
d_p = particle diameter, μm
d_{pg} = geometric mean diameter, μm
k = cluster number cutoff in discrete size spectrum
k_B = Boltzmann constant
k_A = reaction rate constant, s^{-1}
L = length of reactor, cm
M_p = particle mass concentration, g/cm^3
M_s = seed particle mass concentration, g/cm^3
M_w = mass of monomer deposited on wall, g/s
m_w = molecular weight, g/mol
m_m = monomer mass, g
N_{AV} = Avogadro's number, cm^{-3}
N_f = total number concentration of particles, particles/cm^3
N_{J0} = number concentration of homogeneously nucleated particles in the absence of seed particles, particles/cm^3
N_m = monomer number concentration, particles/cm^3
N_p = particle number concentration, particles /cm^3
N_s = seed particle number concentration, particles/cm^3
r = radial position, cm
R_g = gas constant
R = pipe radius, cm
Q_s = flow rate of carrier gas for generating seed particles, cm^3/s
T = absolute temperature, K
t = time, s
u = flow velocity of carrier gas, cm/s
u_{av} = average flow rate of gas, cm/s
v = particle volume, cm^3
v_m = monomer volume, cm^3
z = length from inlet of furnace, cm

Greek letters

α = thermal diffusion coefficient, cm^2/s
$\beta(v, v')$ = Brownian coagulation rate function for two particles of volume v and v', cm^3/s
ρ_p = particle density, g/cm^3
ρ = density of carrier gas, g/cm^3
σ_g = geometric standard deviation

Subscript

s = seed
m = monomer
p = particle

Literature Cited

Friedlander, S. K., *Smoke, Dust and Haze,* Wiley, New York (1977).
Fuchs, N. A., *The Mechanics of Aerosols,* Pergamon Press, Oxford (1964).

Kanai, T., H. Komiyama, and H. Inoue, "TiO_2 Particles by Chemical Vapor Deposition-Particle Formation Mechanism and Chemical Kinetics," *Kagaku Kougaku Ronbunshu*, **11**, 317 (1985).
Nguyen, H. V., K. Okuyama, T. Mimura, Y. Kousaka, R. C. Flagan, and J. H. Seinfeld, "Homogenous and Heterogeneous Nucleation in a Laminar Flow Aerosol Generator," *J. Colloid Interface Sci.*, **119**, 491 (1987).
Okuyama, K., Y. Kousaka, and K. Hayashi, "Change in Size Distribution of Ultrafine Aerosol Particles Undergoing Brownian Coagulation," *J. Colloid Interface Sci.*, **101**, 98 (1984).
Okuyama, K., Y. Kousaka, N. Tohge, S. Yamamoto, J. J. Wu, R. C. Flagan, and J. H. Seinfeld, "Production of Ultrafine Metal Oxide Particles by Thermal Decomposition of Metal Alkoxide Vapor," *AIChE J.*, **32**, 2010 (1986).
Okuyama, K., J. T. Jeung, Y. Kousaka, H. V. Nguyen, J. J. Wu, and R. C. Flagan, "Experimental Control of Ultrafine TiO_2 Particle Generation from the Thermal Decomposition of Titanium Tetraisopropoxide Vapor," *Chem. Eng. Sci.*, **44**, 1369 (1989).
Seinfeld, J. H., *Atmospheric Chemistry and Physics of Air Pollution*, Wiley-Interscience, New York (1986).
Warren, D. R., K. Okuyama, Y. Kousaka, J. H. Seinfeld, and R. C. Flagan, "Homogeneous Nucleation in Supersaturated Vapor Containing Foreign Seed Aerosol," *J. Colloid Interface Sci.*, **116**, 563 (1987).
Wu, J. J., and R. C. Flagan, "Submicron Silicon Powder Production in an Aerosol Reactor," *Appl. Phys. Lett.*, **49**, 82 (1986).
——— "A Discrete-Sectional Solution to the Aerosol Dynamic Equation," *J. Colloid Interface Sci.*, **123**, 339 (1988).
Wu, J. J., H. V. Nguyen, R. C. Flagan, K. Okuyama, and Y. Kousaka, "Evaluation and Control of Particle Properties in Aerosol Reactors," *AIChE J.*, **34**, 1249 (1988).

Appendix

Figure A1 shows experimental data on the thermal decomposition rate k_A against the reciprocal of the temperature T. The solid line indicates the experimental relation obtained by Kanai et al. (1985). From these results, the thermal decomposition rate constant was expressed as

$$k_A = k_0 \exp(-E/R_g T), \quad s^{-1}$$

where

$$k_0 = 3.96 \times 10^5\ s^{-1}, \quad E = 7.05 \times 10^4\ J \cdot mol^{-1}.$$

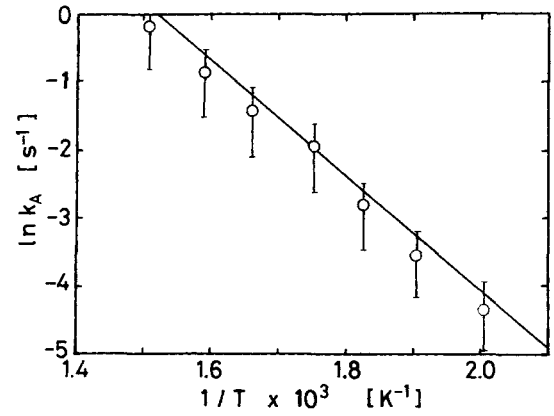

Figure A1. Thermal decomposition rate of TTIP vapor.

Manuscript received June 29, 1989, and revision received Jan. 3, 1990.